Surface & Coatings Technology 268 (2015) 209–215

Contents lists available at ScienceDirect

Surface & Coatings Technology

journal homepage: www.elsevier.com/locate/surfcoat

Effect of the initial particle size distribution on the properties of suspension plasma sprayed Al_2O_3–TiO_2 coatings

M. Vicent [a,*], E. Bannier [a], P. Carpio [a], E. Rayón [b], R. Benavente [b], M.D. Salvador [b], E. Sánchez [a]

[a] Instituto de Tecnología Cerámica (ITC), Asociación de Investigación las Industrias Cerámicas (AICE), Universitat Jaume I (UJI), Av. Vicent Sos Baynat s/n, Castellón 12006, Spain
[b] Instituto de Tecnología de Materiales (ITM), Universitat Politècnica de València (UPV), Camino de Vera s/n, 46022 Valencia, Spain

ARTICLE INFO

Available online 13 December 2014

Keywords:
Suspension plasma spraying
Alumina–titania
Microstructure
Nanoindentation

ABSTRACT

Al_2O_3–TiO_2 coatings have been deposited by atmospheric plasma spraying from agglomerated, nanostructured powders showing better properties than those of their conventional (microstructured) counterparts. These nanostructured coatings can be also obtained by suspension plasma spraying however the research on suspension plasma sprayed Al_2O_3–TiO_2 is still scarce. Consequently, it is crucial to study the effect of the suspension characteristics on the coating properties and to optimize the deposition process.
In this work, Al_2O_3–13 wt.% TiO_2 tribological coatings were successfully deposited by suspension plasma spraying from three different feedstocks: a nanometric suspension and two bimodal suspensions with different solid contents made up of titania nanoparticles and alumina submicron-sized particles. The coating microstructure and phase composition were characterized using scanning electron microscopy and X-ray diffraction analysis. Moreover, nanoindentation technique was used to determine the nanomechanical properties of coatings.
The influence of the feed suspension characteristics on the final coating quality was analyzed. Findings showed that similar microstructures and phases were developed after depositing the different feedstocks. In addition suspension feedstock made up of nanoparticles resulted in a coating with better mechanical properties. However the use of submicron-sized particles in the suspension feedstocks gives rise to some technical and economic advantages in the process which should be taken into account when a suspension plasma spraying process is to be set up.

1. Introduction

A possible way to obtain nanostructured coatings by thermal spraying consists of using a carrier liquid instead of a carrier gas to inject the nanoparticles in the plasma plume [1–5]. This technique is known as suspension plasma spraying (SPS) and differs significantly from conventional atmospheric plasma spraying (APS) since the suspension is fragmented into droplets and the liquid phase vaporizes before the solid feedstock is processed [6,7]. This novel technique has recently undergone an extensive development, leading to the deposition of nanostructured coatings with unique properties and new functionalities [8–11].

Among the materials usually deposited by plasma spraying, alumina-based coatings show probably the most versatile fields of application [12]. Alumina is commonly used as an electrical insulator coating due to its high dielectric strength and its hardness and chemical stability even at very high temperatures. However, its lack of toughness and flaw tolerance constrain some properties such as thermal shock resistance. Still, Al_2O_3-based coatings are widely used for wear, corrosion or erosion protection components. In such coatings, alumina is mixed with other oxides to enhance its properties. It has been shown that the addition of TiO_2 improves the coating fracture toughness in conventional APS [12]. Indeed Al_2O_3–TiO_2 coatings obtained by APS from both conventional or nanostructured, agglomerated feedstock powders have been extensively studied [13–17]. In all the previous research of the authors Al_2O_3–TiO_2 coatings deposited from nanopowders have shown very promising bonding strength and wear resistance compared to coatings produced with conventional feedstock [18]. Moreover, the Al_2O_3–TiO_2 mixture with 13 wt.% of TiO_2 showed the best wear resistance among all the nanostructured Al_2O_3–TiO_2 coatings [19].

With regard to the phases appearing in coatings from alumina feedstocks, Toma et al. [20] observed that a higher amount of α-Al_2O_3 was obtained in SPS coatings when compared with APS coatings. These authors suggested two sources of α-phase in the coating: partially melted α-phase feedstock particles and secondary α-phase formed as a result of substrate heating. Darut et al. also confirmed the high amount of α-phase in SPS coatings obtained from alcoholic suspensions of

* Corresponding author at: Instituto de Tecnología Cerámica, Campus Universitario Riu Sec. Av. Sos Baynat s/n, 12006 Castellón, Spain. Tel.: +34 964342424; fax: +34 964342425.
E-mail addresses: monica.vicent@itc.uji.es (M. Vicent), emilie.bannier@itc.uji.es (E. Bannier), pablo.carpio@itc.uji.es (P. Carpio), emraen@upvnet.upv.es (E. Rayón), rutbmr@upvnet.upv.es (R. Benavente), dsalva@mcm.upv.es (M.D. Salvador), enrique.sanchez@itc.uji.es (E. Sánchez).

http://dx.doi.org/10.1016/j.surfcoat.2014.12.010
0257-8972/

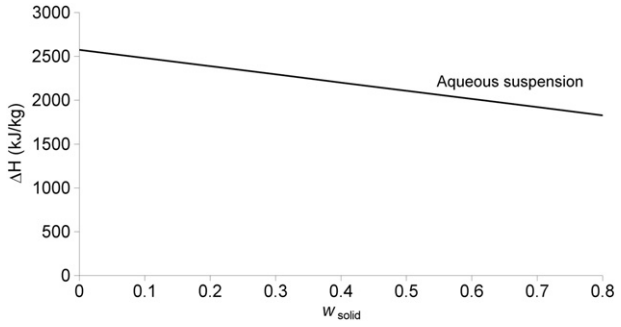

Fig. 1. Plot of the power required to plasma-spray water suspensions of alumina:titania (87:13 weight ratio) by SPS as a function of solid content of suspension feedstock (an estimate by the authors).

submicron-sized α-phase alumina [21]. However these authors pointed out that α-phase presence was probably not mainly due to partially-melted particles as encountered in APS process because most of the coating microstructure exhibited well melted and flattened particles. In this same paper, authors showed that the higher the TiO_2 content the higher the Al_xTiO_y compound content in the coatings. In a recent paper by the authors of the present work, the formation of tialite phase in a SPS coating obtained from aqueous suspension of nano-sized Al_2O_3–13 wt.% TiO_2 was shown while the relative contribution of pre- or post-deposition steps to tialite formation is still unclear [22].

On the other hand in SPS process ethanol has been more extensively used as suspension solvent due to its lower vaporization heat but water is preferable for sustainability and economic reasons [23]. However as the vaporization heat of water is high when higher solid concentration is used in the suspension feedstock an energy-saving effect can be expected. This benefit relates to energy consumption associated to water vaporization during plasma heating. Fig. 1 plots an estimate by the authors of the total enthalpy, ΔH_{total} which means the total energy required to vaporize water as well as to melt a given solid mixture (alumina:titania in a weight ratio of 87:13) versus solid content represented as the solid mass fraction (w_{solid}) present in the suspension feedstock [24,25]. Despite the solid fusion enthalpy increases when suspension solid content rises the enthalpy for vaporizing water compensates and overcomes this fusion enthalpy. Nevertheless although higher solid content feedstocks can be desirable in terms of deposition efficiency this solid content must be optimized to avoid clogging during injection as well as incomplete particle melting inside plasma torch.

With regard to particle size in the suspension feedstock, SPS technology ranges from few tenths of nanometers to few micrometers. When nanoparticles are used a much higher tendency to agglomerate is observed. Besides the particle melting in plasma torch is also deeply affected by the particle size distribution. Thus excessively small particles do not flatten so effectively while large particles and agglomerates display higher tendency to remain partly unmelted [2]. Few attempts have been made to use feedstock mixtures of different particle size distributions, e.g., submicron-nano sized particles despite their many potential advantages. The use of such bimodal distribution in the feedstock suspension can give rise to significant benefits during the suspension processing, i.e., higher solid content and lower viscosity leading to better feeding in the plasma torch along with higher deposition efficiency [26]. Besides some coatings properties can be improved when using bimodal feedstock as recently reported for APS coatings [8,9]. However, the use of these bimodal powders has hardly been treated in SPS literature.

Standard SPS process results in thinner coatings than those obtained by conventional APS process. As a consequence it has been successfully proved that nanoindentation technique is a more feasible method than conventional microindentation for the mechanical characterization of such layers. However, the amount of papers dealing with the use of nanoindentation method to characterize SPS layers is still very scarce [27].

From the above it can be inferred that the research on Al_2O_3–TiO_2 coatings by SPS is in some way incipient. Consequently, it is necessary to study the effect of the characteristics of the feedstock on the final coating microstructure and properties in SPS Al_2O_3–TiO_2 coatings. In addition, the use of submicron-sized particles in SPS feedstocks instead of nano-sized particles can result in significant benefits in terms of suspension feedstock processing while the final coating properties can be in large extent preserved. Also, increasing the solid content in SPS aqueous suspensions remains still a challenge. For these reasons this work aims at depositing Al_2O_3–13 wt.% TiO_2 tribological coatings by SPS from three different feedstocks: a nanometric suspension and two bimodal suspensions with different solid contents made up of titania nanoparticles and alumina submicron-sized particles. The coatings microstructure and phase composition were characterized using scanning electron microscopy and X-ray diffraction analysis. Nanoindentation technique was used to determine the coatings nanomechanical properties. Finally an estimate of energy saving associated with increasing solid content in the suspension feedstock is also included.

2. Materials and methods

2.1. Feedstock preparation

Two commercial nanopowder suspensions of alumina and titania (VP Disp. W630X and AERODISP® W740X respectively, Degussa-Evonik, Germany), a submicron-sized powder of alumina (Condea-Ceralox HPA-0.5, Sasol, USA) and a nanopowder of titania (AEROXIDE® P25, Degussa-Evonik, Germany) were used as raw materials. These materials have been fully characterized in previous works [28–30]. Table 1 shows the main characteristics of the suspensions and powders used to prepare the different feedstocks.

First, a 10 vol.% of 87 wt.% Al_2O_3–13 wt.% TiO_2 nanosuspension was prepared by mixing both commercial suspensions [4,28]. This

Table 1
Main characteristics of the commercial suspensions and powders as provided by the suppliers.

Reference	Suspensions						
	Suspension type	Main crystalline phases	Solid content (wt.%)	pH	Viscosity (mPa · s)	Mean aggregate size (nm)	Density at 20 °C (g/cm^3)
AERODISP VP W630X	Nano-Al_2O_3	Transition aluminas (δ- and γ-Al_2O_3)	30.0 ± 0.1	3.0–5.0	≤2000	140	1.27
AERODISP W740X	Nano-TiO_2	Anatase Rutile	40.0 ± 0.1	5.0–7.0	≤1000	≤100	1.41

Reference	Powders					
	Powder type	Main crystalline phases	Average primary particle size (nm)	Specific surface area (m^2/g)	pH in 4% dispersion	Purity (wt.%)
Condea	Submicron-Al_2O_3	α-Al_2O_3	350	9.5 ± 0.5	–	99.5
P25	Nano-TiO_2	Anatase Rutile	21	50 ± 15	3.5–4.5	99.5

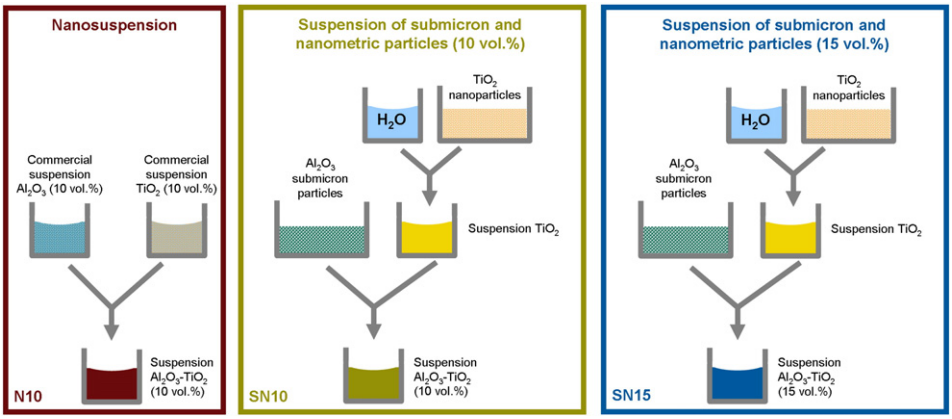

Fig. 2. Flow diagram describing the suspension preparation routes followed to obtain the three suspension feedstocks as well as references adopted.

suspension was referenced as N10. Secondly, on the basis of the effect of suspension solid content on plasma-spray deposition as set out above two suspensions with different solid contents were studied. Thus one 10 vol.% and one 15 vol.% of 87 wt.% Al_2O_3–13 wt.% TiO_2 submicron-nano-sized suspensions were prepared by dispersing nano-sized titania particles and submicron-sized alumina particles in water [30]. These suspensions were referenced as SN10 and SN15 respectively. A commercial polyacrylic acid-based polyelectrolyte (DURAMAX™ D-3005, Rohm & Haas, USA) was used as deflocculant [29–32]. In both cases, stable, well-dispersed and low-viscosity suspensions were obtained, following the methodology described elsewhere [4,28–32]. Fig. 2 details a flow diagram describing the suspension preparation routes followed to obtain the three suspension feedstocks. Rheological behavior of all the prepared suspensions was previously determined using a rheometer, demonstrating that the incorporation of submicron-sized particles leads to a significant reduction of viscosity, as expected for the lower surface area of those particles [31]. Also in previous research of the authors the stability of these three feedstocks was proven [4,28–32].

Stainless steel (AISI 304) disks have been used as substrates (25 mm in diameter and 10 mm in thickness). Before deposition, the substrates were grit blasted with corundum (Metcolite VF, Sulzer Metco, Switzerland) at a pressure of 4.2 bar and cleaned with ethanol.

2.2. Coating deposition

Coatings were deposited by plasma spraying with a monocathode torch (F4-MB, Sulzer Metco, Switzerland) with a 6 mm internal diameter anode operated by a robot (IRB 1400, ABB, Switzerland).

First of all, the substrates were mounted on a rotating device and up to 6 samples were coated simultaneously and were preheated between 350 °C and 400 °C to enhance coating adhesion. The preheating was carried out using the same torch and the parameters are shown in Table 2. Then, the suspensions were injected using a SPS system developed by the Institute for Ceramic Technology (Instituto de Tecnología Cerámica, ITC) described in Fig. 3. This system is formed by two pressurized containers which force the liquid to flow through the injector of 150 μm average diameter. A filter was used to remove agglomerates larger than 75 μm and possible contaminations. Main plasma spraying parameters are also given in Table 2. For all coatings suspension feedrate was 27 ml/min.

2.3. Coating characterization techniques

X-ray diffraction patterns were collected to identify crystalline phases in coating samples (Theta-Theta D8 Advance, Bruker, Germany). The microstructure was analyzed on polished cross-sections using a SEM microscope (JSM6300, Jeol. Japan). Porosity and amount of partially melted areas were then determined by image analysis from SEM pictures as set out in previous research [33]. Magnification pictures of 5000× were used and an average of 10 images for each determination (porosity or partially melted areas) and coating was carried out. Nevertheless it is worthwhile mentioning that when nanoparticles are used SEM technique shows serious constrains to assess too small porosity [34]. Finally, elemental analysis was performed in SEM using energy dispersive X-rays analysis (EDX).

Coating's hardness (H) and elastic modulus (E) were measured with a nanoindenter (G-200, Agilent Technology, USA) using a Berkovich diamond tip. The area function of the indenter was previously calibrated with fused silica as a reference material. A 25-indentation array was performed at 2000 nm constant depth on arbitrary zones of the cross-section of coating, assuring that a representative zone of melted and partially melted material was analyzed. The stiffness was obtained by using the Continuous Stiffness Measurement (CSM) method that permits to calculate the hardness and modulus profiles in depth. Subsequently, the average values of hardness and elastic modulus were determined for a depth ranging from 100 to 200 nm. More details of this procedure can be found in previous research [23,27].

3. Results and discussion

3.1. Coating microstructure

Fig. 4 shows the cross-sectional SEM micrographs of the as-sprayed coatings obtained from the three different feedstocks. The thickness of the coatings ranged from 30 to 55 μm. All the coatings displayed a microstructure formed by melted and partially melted areas (marked PMn in coatings from nano-structured feedstock and marked PMs in coatings from submicron-structured feedstocks) as reported elsewhere [20,22]. This microstructure develops because after the liquid is evaporated the resulting particles or agglomerates may thus be heated, partly melted, or melted, yielding the end coating. Overall no significant

Table 2
Main SPS parameters.

SPS steps	Ar (l/min)	H_2 (l/min)	Arc intensity (A)	Spraying distance (mm)	Spraying velocity (m/s)	Suspension feed rate (ml/min)	Injector diameter (μm)
Pre-heating	35	12	600	100	–	–	–
Spraying	37	8	700	30	1	27	150

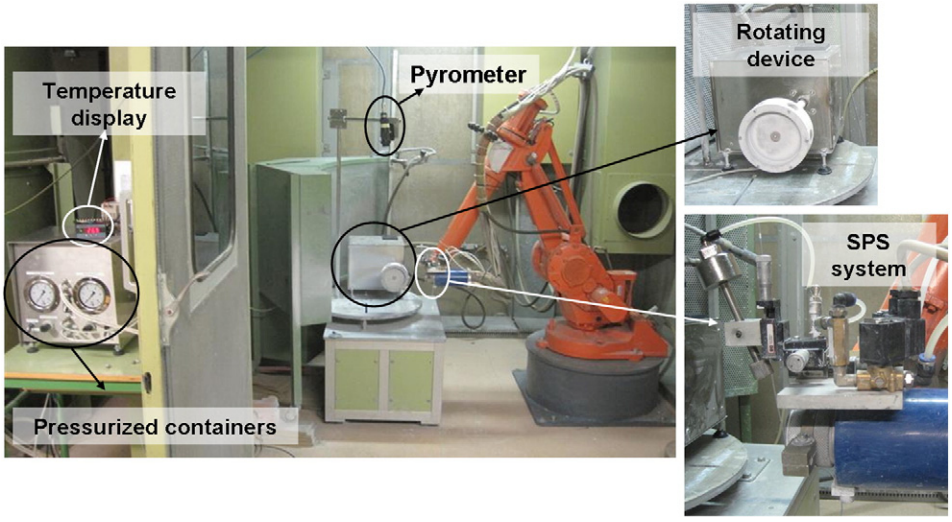

Fig. 3. Suspension plasma spraying equipment.

differences were found in the coatings microstructure by introducing submicron-sized particles in the starting suspension, but as expected this submicron-sized particles addition leads to the presence of larger particles in partially melted areas of the coating (SN10 and SN15). Moreover, it should be noted that the increase of suspension concentration (from SN10 to SN15) did not change the microstructure of the resulting coating but allowed thicker coatings to be obtained (from 30 to 55 μm) giving rise to an improvement of process efficiency.

Porosity and amount of partially melted areas in the three as-sprayed coatings are shown in Table 3. Firstly the three coatings showed a significant as well as quite similar amount of partially melted areas. These values are consistent with those reported in the literature on

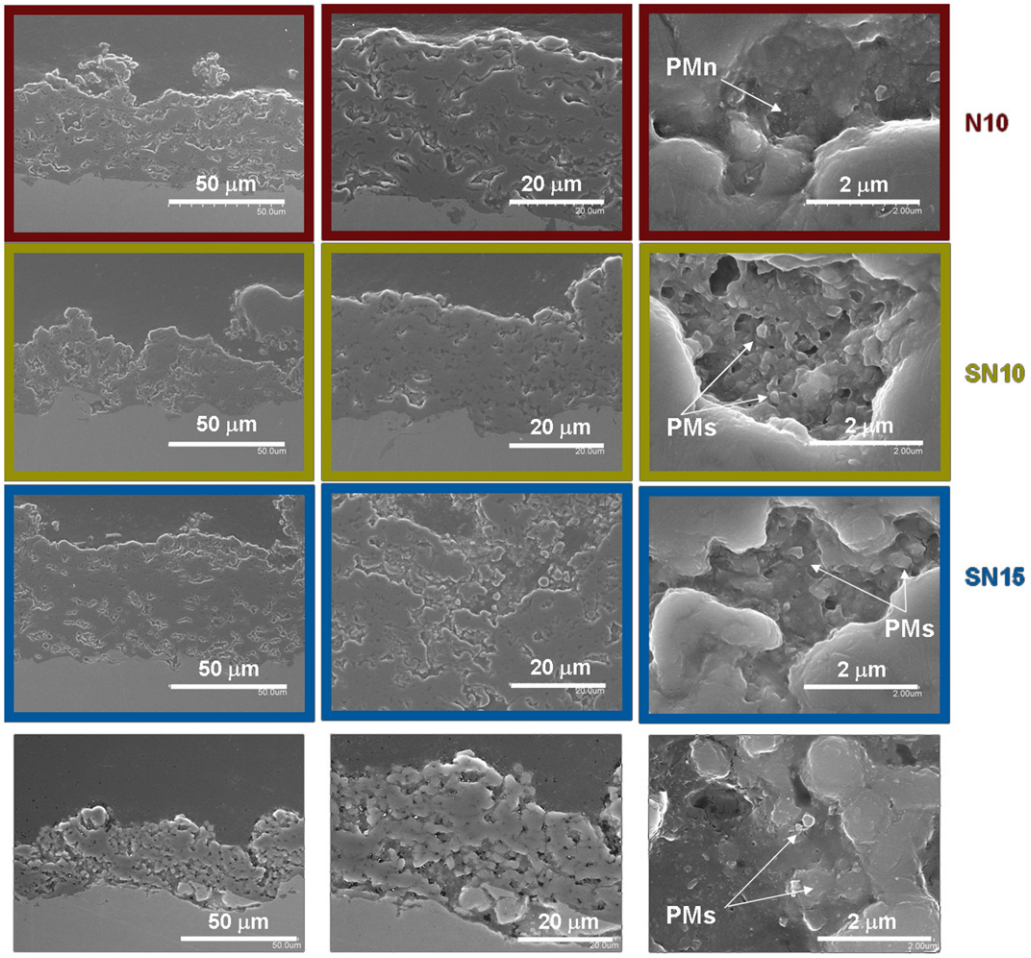

Fig. 4. SEM micrographs at three magnifications of coatings obtained from N10, SN10 and SN15 as well as from N10-aged (marked PMn: partially melted nanoparticles and PMs: partially melted submicron-sized particles).

Table 3
Porosity and amount of partially melted areas determined by SEM of the coatings obtained from the as-prepared suspensions as well as from the aged N10 suspension.

Coating sample	% of partially melted areas	% void content	% void content in the partially melted areas
N10	16 ± 6	0.3 ± 0.3	1 ± 1
SN10	19 ± 6	0.2 ± 0.3	2 ± 1
SN15	19 ± 3	0.3 ± 0.3	7 ± 1
N10-aged	35 ± 8	0.9 ± 0.3	7 ± 1

SPS coatings [2,33]. The similarity in the amount of partially melted areas can be due to the fact that the same spraying distance was used for the three coatings since as reported elsewhere when nanoparticle suspensions are used as feedstocks the amount of partially melted areas are quite sensitive to the spraying distance [33]. Secondly, very little porosity was detected in the three coatings. Nevertheless, it should be noted that the data scattering value obtained was of the same magnitude as the measured data as a consequence of the lack of resolution of the SEM technique when very tiny pores are present as reported elsewhere [34]. More interestingly the measurable coating porosity by SEM technique in the partially melted areas increases as the concentration in the suspension feedstock rises (from SN10 to SN15 coating). This is probably due to the higher presence of agglomerates in the partially melted areas of SN15 coating as a consequence of higher agglomeration tendency of the more concentrated SN15 suspension. To confirm this assumption N10 suspension was allowed to age after 7 days in order to enhance the presence of unstable agglomerates. This suspension (referenced N10-aged) was plasma sprayed in the same conditions as the other three suspensions. Fig. 5 shows both suspensions (N10 and N10-aged) flow curves. N10 suspension exhibited Newtonian behavior with very low viscosity. However, the N10-aged suspension viscosity significantly increased and a large thixotropy area appeared, evidencing the destabilization of the stable (well-dispersed) N10 suspension [30]. As seen in Table 3 the unstable agglomerates built up in the aged suspension result in an increase of partially melted areas in the coating as well as a significant source of measurable, large voids.

To assess the homogeneity of alumina–titania distribution in the coating EDX analysis was carried out on the three coatings (N10, SN10 and SN15). For the sake of simplicity Fig. 6 shows only the analysis corresponding to N10 coating since similar analyses were carried out on the other two samples. Dark dots refer to alumina phases and the whitish ones to titania phases. Overall as it can be observed alumina and titania phases are homogeneously deposited throughout the coating. This compositional homogeneity in the coatings contrasts with that obtained by other works using conventional or nanostructured alumina–titania APS feedstocks which give rise to splats with heterogeneous phase compositional distribution [35,36]. Thus TiO_2 has been well trapped as solute in the alumina matrix. Moreover as reported in previous research by the authors, BSE micrographs on Al_2O_3–13 wt.% TiO_2 coating revealed zones with different concentration of Ti or Al probably due to the presence of different crystalline phases [22]. These findings indicate that the preparation of the suspension feedstocks is crucial to obtain a homogeneous distribution of the compounds in the final SPS coating [4,31,32]. If this preparation is adequate the characteristics of the suspension feedstock, i.e., solid concentration or particle size distribution do not seem to affect on coating homogeneity in terms of phases distribution.

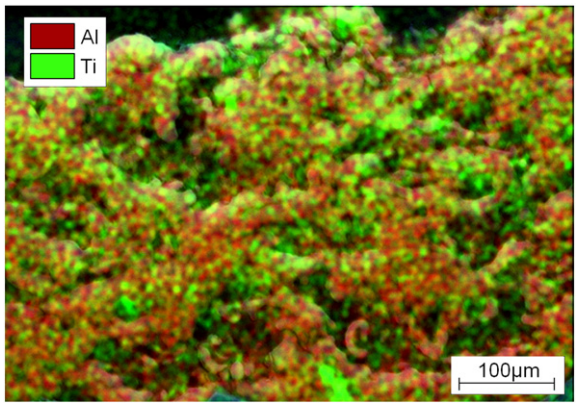

Fig. 6. EDX analysis of coating obtained from N10.

Finally, XRD patterns of all coatings are shown in Fig. 7. As it can be observed the alumina found in the three coating is mainly present as corundum and gamma alumina, independently of feed material phases since nanometric alumina is formed by transition phases (δ- and γ-Al_2O_3) and submicron-sized alumina is exclusively corundum (α-Al_2O_3). These findings seem to confirm the information reported in the literature concerning α-phase formation: partially melted α-phase feedstock particles and secondary α-phase formed as a result of substrate heating [20]. For this reason, the amount of preserved corundum grows in the coatings containing submicron-sized particles (samples SN10 and SN15). In respect of titania, most of the initial phase (an anatase:rutile ratio of approximately 3:1) reacts with alumina during the deposition process, leading to the formation of aluminium titanate (tialite). This finding confirms the intimate mixture of compounds in the starting suspensions in a SPS process since similar compositions of alumina–titania sprayed in powder form (APS process) react in less extent to form these titanate compounds [32]. The formation of tialite phase in SPS coating obtained from a suspension feedstock made up of Al_2O_3–13 wt.% TiO_2 has been previously reported in the literature [21,22]. Nevertheless if the formation of this crystalline phase takes mainly place by heating during torch travel or on the deposited layer is still unclear. The short spraying distances involved in SPS process can favor that the reaction occurs once the layer has been deposited. However further research in necessary to prove this statement.

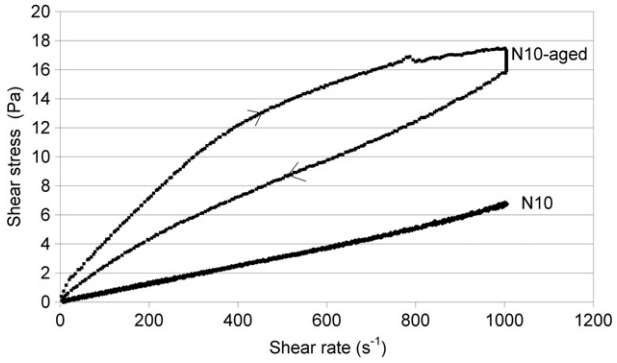

Fig. 5. Flow curves of the as-prepared N10 suspension and N10-aged suspension.

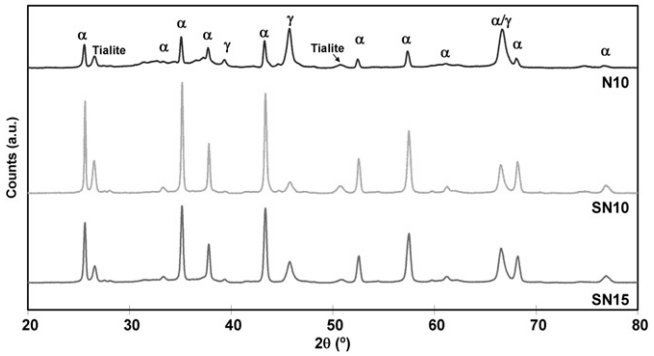

Fig. 7. XRD patterns of coatings obtained from N10, SN10 and SN15.

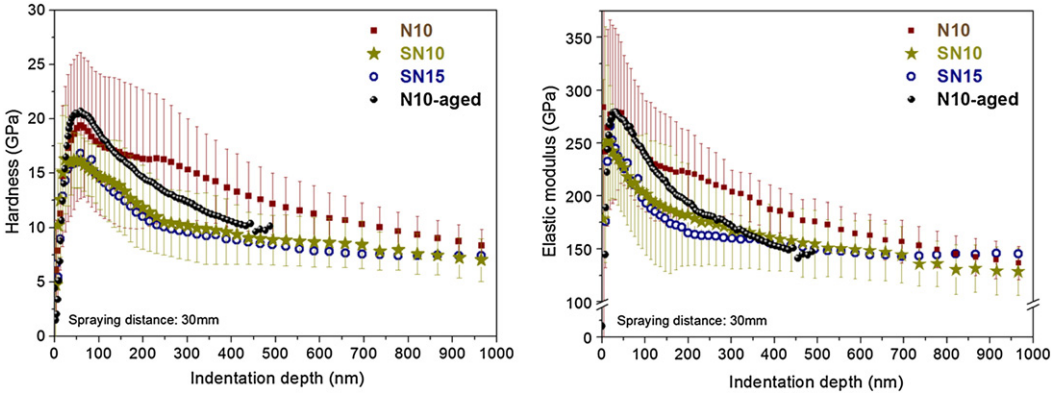

Fig. 8. Hardness and elastic modulus obtained on coatings by nanoindentation (samples: N10, SN10. SN15 and N10-aged).

3.2. Coating mechanical properties

The coating's hardness (H) and elastic modulus (E) were measured by nanoindentation. As described above, all indentations were performed at 2000 nm in depth randomly positioned on several zones of sample. Fig. 8 shows the mean and standard deviation hardness and elastic modulus profiles obtained for each analyzed coating obtained from the as-prepared suspensions (N10, SN10, SN15). These curves revealed two main characteristic behaviors; (i) at low penetration depths (below 300 nm for H and 100 nm for E), hardness and elastic modulus ranged from 15 to 29 GPa and 250 to 280 GPa respectively. At higher loads the mechanical response tended to decrease. Furthermore, (ii) the data scattering was higher for the lower range of depth. These results indicate that at a lower range of penetration depth the true material's H and E are revealed. That is, the melted zones achieve the highest values and the partially melted areas the lowest leading to the high data scattering observed. However, at a higher penetration depth the porosity, which is the major effect affecting on the softer, partially melted material, the indentation size effect, the activated microcracks and other plastic mechanism are responsible for the diminution of mechanical features.

In this study, the comparative analysis using the H and E mean values acquired at low penetration range of depth was the main focus, because these results allow more realistic features of the projected material (alumina–titania) to be determined without taking into account microstructural defects that could be removed o diminished in incoming works. This was the reason why results were averaged between 100 and 200 nm. Table 4 summarizes the averaged H and E values for each deposited coating acquired by nanoindentation.

These results reveal that mechanical properties are significantly better (around 30% higher) for the coating prepared from nanoparticles (N10). Thus this finding confirms previous research when nanostructured feedstocks were used in APS processes [31,32,37]. As the literature states that submicron-structured matrices contained in coatings obtained from nanostructured feedstocks result in coatings with better mechanical properties provided that the amount and poor cohesion of partially melted zones do not compensate the enhancement matrix effect. However, although the number of papers about mechanical properties in alumina–titania coatings, obtained from nanostructured feedstocks by APS process is abundant, no papers on SPS coatings from nano- or submicron-sized alumina–titania feedstocks addressing mechanical properties have been found. In one previous paper similar comparison of nanoindentation mechanical properties in alumina–titania coatings obtained from nano- and submicron-sized suspensions was carried out but the authors produced the coatings by HVSFS (High Velocity Suspension Flame Spraying) [38]. Nevertheless this paper highlights an important issue in suspension sprayed coatings since the authors did not find differences in the mechanical properties of the coatings sprayed with nano- or submicron-sized feedstocks owing to the agglomeration state of nanoparticles in the suspension feedstock. In the present research the dispersion and stabilization of the suspension feedstocks were previously set out [29,30]. For this reason the effect of nanoparticles on mechanical properties in N10 coating could be fully developed. To confirm this statement nanoindentation test on the N10-aged coating obtained as set out in previous section was also acquired. Results of this test are also displayed in Fig. 8. As this figure reveals, the effect of the agglomeration provoked in N10-aged suspension is reflected in the mechanical behavior of N10-aged coating. Hence, H and E curves showed an intermediate profile development between N10 and SN10/SN15 coatings, as a consequence of the much higher content of partially melted areas built up from the agglomerated feedstock suspension of N10-aged coating in comparison with N10 coating. As set out above the destabilization of the nanoparticle suspension feedstock gives rise to an impaired coating microstructure made up of higher amount of partially melted areas containing coarser pores. Consequently decreasing averaged values of H and E in the coating were obtained which were closer to those of the SN coatings. Nevertheless the values of H and E mechanical properties could not be averaged and included in Table 4 due to the high data scattering found in this coating sample.

Previous research on nanoindentation in SPS coatings obtained from nanoparticle suspension feedstocks of other oxides such as YSZ (yttria-stabilized zirconia) or titania highlighted the enhanced mechanical properties found when nanoparticles suspensions were used as a consequence of the ultrafine character of SPS coating splats [23,27]. These papers also showed the mechanical weakening effect of the partially melted areas which appear in more or less extent in SPS coatings. Further research is still necessary to confirm these preliminary findings, and more importantly, to establish a clear relation between coating microstructure and mechanical properties.

Finally, regarding SN coatings, an increase of suspension concentration in the range addressed in this research did not modify mechanical properties of the coatings what could be considered, in principle, a positive effect if an optimization of the solid concentration in the feedstock suspension is targeted as a consequence of the possible technical and economic benefits set out above.

Overall the effect of increasing of the solid concentration in the suspension feedstock has not proven to show a clear effect on coating microstructure and properties, at least in the variation range addressed in this preliminary research. For this reason, further research is now in

Table 4
Hardness and modulus averaged values of coatings.

Sample	Hardness (GPa)	Elastic modulus (GPa)
N10	16 ± 2	225 ± 20
SN10	13 ± 2	178 ± 21
SN15	12 ± 2	175 ± 18

progress in order to better analyze in an isolated way the effect of solid content and the agglomeration (stabilization) degree of the suspension feedstock. To achieve this objective, increasing solid concentration suspensions of submicron-sized alumina particles will be prepared and the stabilization degree of these suspensions will be conveniently modified. The effect of the spraying distance during plasma spraying deposition will also be taken into account due to its great effect on the amount of partially melted areas in the coatings.

4. Conclusions

Al_2O_3–TiO_2 coatings were successfully deposited by SPS from suspensions in which particle size (nano- and submicron-sized particles) and solid concentration were varied. Findings showed that similar microstructures made up of melted matrices and partially melted zones were obtained. The alumina found in the coatings is mainly present as corundum and gamma alumina. In respect of titania, most of the initial phase reacts with alumina during the deposition process, leading to the formation of aluminium titanate (tialite). In addition the developed alumina and titania phases were homogenously distributed throughout the different coatings. On the other hand suspension feedstock made up of nanoparticles resulted in a coating with better mechanical properties than those obtained from submicron-sized particles. However when the nanoparticle suspension feedstock was destabilized impaired microstructure containing a higher amount of partially-melted areas with coarse pores was obtained. This impaired microstructure led to worse mechanical properties which were closer to those of the coatings obtained from submicron-sized particles. No effect of solid concentration in submicron-sized feedstocks on coating mechanical properties was observed for the solid concentration variation and plasma spraying conditions used in this research. However the use of submicron-sized particles to obtain suspension feedstocks with high solid concentration proved to give rise to some technical (improved processability) and economic (lower energy consumption) advantages in the SPS process which should be taken into account when a SPS process is to be set up.

Acknowledgments

This work has been supported by the Spanish Ministry of Science and Innovation (project MAT2012-38364-C03) and it has been co-funded by ERDF (European Regional Development Funds).

References

[1] A.K. Keshri, A. Agarwal, Nanosci. Nanotechnol. Lett. 4 (2012) 228–250.
[2] P. Fauchais, G. Montavon, R.S. Lima, B.R. Marple, J. Phys. D Appl. Phys. 44 (9) (2011) 93001.
[3] B.R. Marple, R.S. Lima, Adv. Appl. Ceram. 106 (5) (2007) 265–275.
[4] E. Sánchez, A. Moreno, M. Vicent, M.D. Salvador, V. Bonache, E. Klyatskina, I. Santacruz, R. Moreno, Surf. Coat. Technol. 205 (4) (2010) 987–992.
[5] E.H. Jordan, M. Gell, Y.H. Sohn, D. Goberman, L. Shaw, S. Jiang, M. Wang, T.D. Xiao, Y. Wang, P. Strutt, Surf. Coat. Technol. 146–147 (2001) 48–54.
[6] L. Pawlowski, Surf. Coat. Technol. 203 (19) (2009) 2807–2829.
[7] R. Vassen, H. Kassner, G. Mauer, D. Stöver, J. Therm. Spray Technol. 19 (1–2) (2010) 219–225.
[8] M. Marr, O. Kesler, J. Therm. Spray Technol. 21 (6) (2012) 1334–1346.
[9] A. Guignard, G. Mauer, R. Vassen, D. Stöver, J. Therm. Spray Technol. 21 (3–4) (2012) 416–424.
[10] G. Mauer, A. Guignard, R. Vassen, Surf. Coat. Technol. 220 (2013) 40–43.
[11] R. Tomaszek, L. Pawlowski, L. Gengembre, J. Laureyns, A. Le Maguer, Surf. Coat. Technol. 201 (16–17) (2007) 7432–7440.
[12] R.B. Heimann, Plasma-Spray Coating, second ed. Wiley–VCH, 2008.
[13] A. Rico, P. Poza, J. Rodríguez, Vacuum 88 (1) (2013) 149–154.
[14] R. Yilmaz, A.O. Kurt, A. Demir, Z. Tatli, J. Eur. Ceram. Soc. 27 (2–3) (2007) 1319–1323.
[15] R. Tomaszek, L. Pawlowski, J. Zdanowski, J. Grimblot, J. Laureyns, Surf. Coat. Technol. 185 (2–3) (2004) 137–149.
[16] S. Guessasma, M. Bounazef, P. Nardin, T. Sahraoui, Ceram. Int. 32 (1) (2006) 13–19.
[17] E.H. Jordan, M. Gell, Y.H. Sohn, D. Goberman, L. Shaw, S. Jiang, M. Wang, T.D. Xiao, Y. Wang, P. Strutt, Mater. Sci. Eng. A 301 (1) (2001) 80–89.
[18] J. Ahn, B. Hwang, E.P. Song, S. Lee, N.J. Kim, Metall. Mater. Trans. A 37 (2006) 1851–1861.
[19] X. Lin, Y. Zeng, S.W. Lee, C. Ding, J. Eur. Ceram. Soc. 24 (2004) 627–634.
[20] F.L. Toma, L.M. Berger, C.C. Stahr, T. Naumann, S. Langner, J. Therm. Spray Technol. 19 (1–2) (2010) 262–274.
[21] G. Darut, E. Klyatskina, S. Valette, P. Carles, A. Denoirjean, G. Montavon, H. Ageorges, F. Segovia, M.D. Salvador, Mater. Lett. 67 (1) (2012) 241–244.
[22] E. Bannier, M. Vicent, E. Rayón, R. Benavente, M.D. Salvador, E. Sánchez, Appl. Surf. Sci. 316 (2014) 141–146.
[23] P. Carpio, E. Rayón, L. Pawlowski, A. Cattini, R. Benavente, E. Bannier, M.D. Salvador, E. Sánchez, Surf. Coat. Technol. 220 (2013) 237–243.
[24] E.M. Levin, C.R. Robbins, H.F. McMordie, Phase Diagrams for Ceramist. Volume I, fifth ed. The American Ceramic Society, Columbus, 1964.
[25] R.H. Perry, C.H. Chilton, Chemical Engineers' Handbook, fifth ed. McGraw–Hill, New York, 1973.
[26] D. Waldbillig, O. Kesler, Surf. Coat. Technol. 203 (15) (2009) 2098–2101.
[27] E. Rayón, V. Bonache, M.D. Salvador, E. Bannier, E. Sánchez, A. Denoirjean, H. Ageorges, Surf. Coat. Technol. 206 (10) (2012) 2655–2660.
[28] M. Vicent, E. Sánchez, T. Molina, M.I. Nieto, R. Moreno, J. Eur. Ceram. Soc. 32 (5) (2012) 1019–1028.
[29] M. Vicent, E. Sánchez, A. Moreno, R. Moreno, J. Eur. Ceram. Soc. 32 (1) (2012) 185–194.
[30] M. Vicent, E. Sánchez, T. Molina, M.I. Nieto, R. Moreno, Ceram. Int. 39 (8) (2013) 9091–9097.
[31] M. Vicent, E. Bannier, R. Benavente, M.D. Salvador, T. Molina, R. Moreno, E. Sánchez, Surf. Coat. Technol. 220 (2013) 74–79.
[32] M. Vicent, E. Bannier, R. Moreno, M.D. Salvador, E. Sánchez, J. Eur. Ceram. Soc. 33 (15–16) (2013) 3313–3324.
[33] P. Carpio, E. Bannier, M.D. Salvador, A. Borrell, R. Moreno, E. Sánchez, Effect of particle size distribution of suspension feedstock on the microstructure and mechanical properties of suspension plasma spraying YSZ coatings, Surf. Coat. Technol. http://dx.doi.org/10.1016/j.surfcoat.2014.08.063
[34] A. Bacciochini, G. Montavon, J. Ilavsky, A. Denoirjean, P. Fauchais, J. Therm. Spray Technol. 19 (2009) 198–206.
[35] R. Venkataraman, S.P. Singh, B. Venkataraman, D.K. Das, L.C. Pathak, S.G. Chowdhury, R.N. Ghosh, D. Ravichandra, G.V.N. Rao, K. Nair, R. Kathirkar, Surf. Coat. Technol. 202 (2008) 5074–5083.
[36] E. Sánchez, E. Bannier, V. Cantavella, M.D. Salvador, E. Klyatskina, J. Morgiel, J. Grzonka, A.R. Boccaccini, J. Therm. Spray Technol. 17 (3) (2008) 329–337.
[37] E. Sánchez, E. Bannier, M. Vicent, A. Moreno, M.D. Salvador, V. Bonache, E. Klyatskina, A.R. Boccaccini, Int. J. Appl. Ceram. Technol. 8 (5) (2011) 1136–1146.
[38] G. Bolelli, V. Cannillo, R. Gadow, A. Killinger, L. Lusvarghi, J. Rauch, M. Romagnoli, Surf. Coat. Technol. 204 (8) (2010) 1163–1179.